

Complete identification of the Parkes half-Jansky sample of GHz peaked spectrum radio galaxies[★]

N. de Vries¹, I. A. G. Snellen¹, R. T. Schilizzi^{1,2}, M. D. Lehnert^{3,4}, and M. N. Bremer⁵

¹ Leiden Observatory, Leiden University, P.O. Box 9513, 2300 RA, Leiden, The Netherlands
e-mail: vriesn@strw.leidenuniv.nl

² International Square Kilometre Array Project office, Postbus 2, 7990 AA, Dwingeloo, The Netherlands

³ Max-Planck-Institut für extraterrestrische Physik (MPE), Postfach 1312, 85741 Garching, Germany

⁴ Laboratoire d'Etudes des Galaxies, Etoiles, Physique et Instrumentation, Observatoire de Paris, 5 Place Jules Janssen, 92195 Meudon, France

⁵ Department of Physics, Bristol University, H H Wills Physics Laboratory, Tyndall Avenue, Bristol BS8 1TL

Received 4 October 2006 / Accepted 15 December 2006

ABSTRACT

Context. Gigahertz Peaked Spectrum (GPS) radio galaxies are generally thought to be the young counterparts of classical extended radio sources. Statistically complete samples of GPS sources are vital for studying the early evolution of radio-loud AGN and the trigger of their nuclear activity. The ‘Parkes half-Jansky’ sample of GPS radio galaxies is such a sample, representing the southern counterpart of the 1998 Stanghellini sample of bright GPS sources.

Aims. As a first step of the investigation of the sample, the host galaxies need to be identified and their redshifts determined.

Methods. Deep *R*-band VLT-FORS1 and ESO 3.6m EFOSC II images and long slit spectra have been taken for the unidentified sources in the sample.

Results. We have identified all twelve previously unknown host galaxies of the radio sources in the sample. Eleven have host galaxies in the range $21.0 < R_C < 23.0$, while one object, PKS J0210+0419, is identified in the near infrared with a galaxy with $K_s = 18.3$. The redshifts of 21 host galaxies have been determined in the range $0.474 < z < 1.539$, bringing the total number of redshifts to 39 (80%). Analysis of the absolute magnitudes of the GPS host galaxies show that at $z > 1$ they are on average a magnitude fainter than classical 3C radio galaxies, as found in earlier studies. However their restframe UV luminosities indicate that there is an extra light contribution from the AGN, or from a population of young stars.

Key words. Galaxies: active – Galaxies: distances and redshifts – Galaxies: photometry

1. Introduction

Gigahertz Peaked Spectrum (GPS) radio sources are among the brightest radio sources in the sky. They are compact objects characterized by a turnover in their radio spectra at about 1 GHz in frequency. Their radio morphologies are small-scale versions of the well known extended Fanaroff & Riley (FR) I/II radio sources, but with a physical extent of only 10-100 pc, well within the central regions of their host galaxies (Stanghellini et al. 1999). To explain the compactness of these sources two scenarios were proposed: (1) these objects are very young radio-loud active galaxies which may evolve into kpc-sized Compact Steep Spectrum (CSS) sources and eventually grow to become

FR I/II, (2) they are ‘frustrated’ radio sources, millions of years old, but confined by a dense interstellar medium (Baum et al. 1990). In recent years compelling evidence has accumulated in favour of the youth scenario. VLBI monitoring of the archetype GPS sources, that began in the early 1980s, has now conclusively shown these sources expand in size, implying source ages of 10^{2-3} years only (Owsianik et al. 1998; Owsianik & Conway 1998; Tschager et al. 2000; Polatidis & Conway 2003), in good agreement with spectral age estimates (Murgia 2003). Recently Vink et al. (2006) have shown that their optical line emission is relatively underluminous, exhibiting a possible trend with radio source age. This is consistent with the fact that the Strömgren sphere should still be expanding in these objects, and that we are witnessing the birth of their narrow emission line regions. If indeed GPS galaxies are young, as now seems to be very likely, they form the key objects to study the early evolution of powerful radio-loud AGN, and the trigger of nuclear activity. In this paper we present

Send offprint requests to: vriesn@strw.leidenuniv.nl

[★] Based on observations collected at the European Southern Observatory Very Large Telescope, Paranal, Chile (ESO prog. ID No. 073.B-0289(B)) and the European Southern Observatory 3.6m Telescope, La Silla, Chile (prog. ID No. 073.B-0289(A)).

new optical observations of a sample of GPS galaxies, aimed at identifying all host galaxies and determining their redshifts. Section 2 defines this sample, section 3 describes the observations, and the results are presented and discussed in Sect. 4.

2. The Parkes half-Jansky sample of GPS galaxies

Snellen et al. (2002) have defined a sample of bright GPS sources in the southern/equatorial sky, representing the counterpart of the sample of Stanghellini et al. (1998), although somewhat deeper. High flux density GPS sources are rare and therefore all sky coverage is needed in order to obtain a statistically significant number of sources. Furthermore, access to large optical telescopes is better for the southern hemisphere, at least for European astronomers. The selection criteria of the sample are described in detail in a previous paper (Snellen et al. 2002). Summarizing, it consists of 49 sources selected from the Parkes multifrequency survey (PKSCAT90, Wright & Otrupcek 1990), with $-40^\circ < \delta < +15^\circ$, $|b| > 20^\circ$ and $S_{2.7\text{GHz}} > 0.5\text{Jy}$. The sample only consists of GPS radio sources associated with galaxies since GPS quasars do not seem to be related to GPS galaxies, despite having similar radio characteristics, and may not be young (e.g. Snellen et al. 1999). Before the current work, 75% of the radio sources had been optically identified with a host galaxy and 40% had known redshifts.

3. Observations

3.1. VLT-FORS1 spectroscopy

Optical long slit spectroscopy was performed on objects in the sample using the European Southern Observatory (ESO) Very Large Telescope (VLT) at Paranal, in Chile, from March to September 2004. All observations were obtained in service mode with the visual and near UV FOcal Reducer and low dispersion Spectrograph (FORS1), using exposure times of 1800 s with the grism GRIS-300V (ESO # 10) in combination with the order separation filter GG 435. The FORS1 has a Tektronix 2048×2048 CCD detector with $24\mu\text{m}$ pixels, resulting in a scale of $0.2''/\text{pixel}$ (with the Standard Resolution collimator) and a slit length of $6.8'$. The grism results in a dispersion of $2.69 \text{ \AA}/\text{pixel}$ and a total wavelength coverage of $4450 - 8650 \text{ \AA}$. The spectra were taken using a slit width of $1.0''$, resulting in a spectral resolution of $\text{FWHM} = 5 \text{ pixels}$ (13 \AA). Usually the slit was oriented near the parallactic angle, unless a second interesting object was located near the GPS galaxy (e.g. a possibly associated companion galaxy). The data reduction was carried out in a standard way using NOAO's IRAF reduction software. One dimensional spectra were extracted by summing in the spatial direction over an aperture as large as the spatial extent of the continuum or the brightest emission line. Acquisition images were taken to center the slit and in addition, for a few sources, to determine their R -band magnitude.

3.2. ESO 3.6m observations

Optical CCD imaging and spectroscopy were also performed using the ESO 3.6m Telescope at La Silla, in Chile, on March

23 and 24, 2004. For all observations we used the ESO Faint Object Spectrograph and Camera (EFOOSC II), which has a 2048×2048 CCD detector with $15\mu\text{m}$ pixels resulting in a scale of $0.157''/\text{pixel}$ and a field size of $5.4' \times 5.4'$. Spectroscopic observations were carried out in long slit mode with a slit width of $1.2''$, using the EFOOSC grism #6, which has a wavelength coverage of $3860 - 8070 \text{ \AA}$ and a dispersion of $137 \text{ \AA}/\text{mm}$ or $2.06 \text{ \AA}/\text{pixel}$. The slit was always oriented near the parallactic angle. The reduction of the spectra was carried out in a similar way to the VLT data.

Photometric observations were carried out in Gunn r -band (EFOOSC filter r#786). The reduction of the images was carried out in a standard way using NOAO's IRAF reduction software. Astrometry was performed using data from the USNO-B1.0 Catalog, extracted with the Vizier catalogue access tool. For each image, catalogued positions of at least ten stars were used. With the IRAF procedure CCMAP, the equatorial coordinates were determined with errors always well within one pixel. Optical identifications were found, within the $1-\sigma$ uncertainty ellipse, for all seven radio sources. Photometry was carried out using the IDL procedure APER with the aperture diameter set to $2.51''$ (16 pixels). The magnitude scale was calibrated using Landolt standard stars, with their Cousins R_C magnitudes converted to Gunn r using the conversion formula from Schombert et al. (1990):

$$r = R_C + 0.280 + 0.038(R_C - I_C) \quad (1)$$

For better comparison with the rest of the sample, we also calculated Cousins R_C magnitudes of the sources by using the unconverted Cousins R_C magnitudes of the standard stars to calibrate our Gunn r data. Since the colors of the sources are unknown, this conversion introduces extra uncertainties. However, these were always found to be small compared to the photometric errors.

3.3. Additional near-infrared photometry

Earlier optical observations of the GPS source PKS J0210+0419 (Snellen et al. 2002), did not result in an identification, with a lower limit of $m_R > 24.1$. We therefore observed this source in K_s -band using the SOFI near-infrared camera on ESO's New Technology Telescope (NTT). SOFI is equipped with a Rockwell 1024×1024 detector that provides images with a pixel scale of $0.288''/\text{pixel}$, and a field of view of about $4.9' \times 4.9'$ (Large Field imaging mode). The SOFI K_s filter has a central wavelength of $2.162 \mu\text{m}$ and a width of $0.275 \mu\text{m}$. Details of the K_s -band observations of PKS J0210+0419 and of other sources in the sample will be published in a following paper, however we present the K_s -band identification and magnitude of PKS J0210+0419 ($K_s = 18.3$) here for completeness.

4. Results and discussion

In total, eleven previously unidentified sources in the sample have been observed in R -band with the ESO 3.6m and VLT telescopes. All were optically identified, with $21.0 < R_C < 23.0$. Including the one identification in K -band

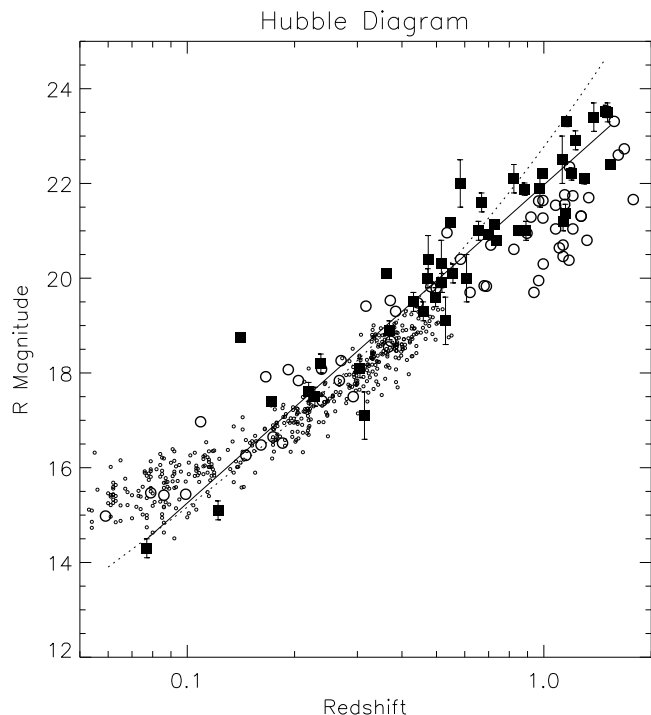


Fig. 1. Cousins R_C Hubble diagram of GPS galaxies (solid squares), 3C galaxies (open circles), and LRGs (small circles). The dotted line is the R -band Hubble relation as derived by Snellen et al. (1996a), the solid line is a linear least squares fit to the current data.

(PKS J0210+0419), this means that the Parkes half-Jansky sample of GPS galaxies is now *completely* identified. Note that we have left one source (PKS J1600–0037) out of our statistical sample, because it is located too close to a 12th magnitude star to make an optical identification possible. Since this is a random occurrence, it does not introduce any selection effects, so the sample will remain statistically complete. The results of the photometric observations are given in Table 1; in column 1 the source name, in column 2 the exposure time, in column 3 the observed Gunn r -band magnitude with its error, and in column 4 the observed or deduced Cousins R_C -band magnitude.

We have also taken deep spectra of 24 objects in total. These have resulted in twenty secure redshifts, based on two or more emission or absorption lines, all in the range $0.474 < z < 1.539$. One spectrum (PKS J1556-0622) resulted in a tentative redshift ($z = 1.195$), based on only one line. We assumed the line to be [OII] 3727 Å, because of the resemblance between this spectrum and those of PKS J2339–0604 and PKS J2212+0152, and the absence of plausible alternatives. A further nine sources in the sample (19%) remain without redshift. The results of the spectroscopic observations are given in the appendix (Table B.2); in column 1 the source name, in column 2 the exposure time, in column 3 the name of the telescope used, in columns 4-7 respectively the name, rest wavelength, observed wavelength and rest-frame equivalent width of the identified spectral features, and in column 8 the derived redshift for each identified spectral feature and

Table 1. Details of the photometric observations.

ESO 3.6m Telescope observations			
Object name	t (s)	m_r	m_{R_C}
PKS J0441–3340	600	22.8 ± 0.4	22.5 ± 0.4
PKS J0913+1454	1200	23.2 ± 0.5	22.9 ± 0.5
PKS J1044–2712	1200	23.1 ± 0.4	22.8 ± 0.4
PKS J1057+0012	1200	22.6 ± 0.3	22.3 ± 0.3
PKS J1109+1043	1200	22.9 ± 0.3	22.6 ± 0.3
PKS J1122–2742	1600	23.3 ± 0.5	23.0 ± 0.5
PKS J1135–0021	60		21.9 ± 0.4
PKS J1648+0242	1200	22.4 ± 0.3	22.1 ± 0.3
ESO VLT observations			
Object name	t (s)	m_{R_C}	
PKS J0401–2921	10	21.0 ± 0.2	
PKS J1345–3015	10	21.2 ± 0.2	
PKS J1352+1107	10	21.0 ± 0.2	
ESO NTT observation			
Object name	t (s)	m_{K_s}	
PKS J0210+0419	450	18.3 ± 0.2	

for each source. All spectra are also shown in the appendix (Fig. B.1).

4.1. R -band Hubble diagram

Now that we have significantly increased the number of GPS galaxies with known redshifts, particularly around redshift $z \sim 1$, it is interesting to review the R -band Hubble relation as previously discussed by Snellen et al. (1996a) and O’Dea et al. (1996). For this purpose we combined our southern/equatorial sample with the northern sample of GPS sources of Stanghellini et al. (1998), excluding all those objects identified with quasars. Spectroscopic observations of two sources from our sample (PKS J1203+0414 and PKS J1506–0919) reveal broad emission lines ($\sim 10^4$ km/s) and non-thermal emission. Technically these sources are now identified as quasars, and have been omitted from the sample. The resulting R -band Hubble diagram of GPS galaxies (solid squares) is shown in Fig. 1. For comparison, 3C radio galaxies (open circles) from a compilation of samples (Best et al. (1997), Eales (1985), and de Koff et al. (1996)) and a subset of the ‘Luminous Red Galaxies’ (LRGs; small circles) sample (Eisenstein et al. 2001) from the Sloan Digital Sky Survey (SDSS) are shown. If necessary, the magnitudes were converted to ‘total magnitudes’ in Cousins R_C . Note the one GPS source (PKS J1604–2223, with $R_C = 18.75$ and $z = 0.141$) that is over two magnitudes fainter than the general population. This is much too faint for a typical powerful AGN host galaxy, for which a number of explanations could be given. Although the source is located in a region with high galactic extinction, it is unlikely that this is the reason for the offset, since the object is also over two magnitudes fainter in K -band (de Vries et al. in prep.) than expected from the K -band Hubble diagram (as presented by Snellen et al. 1996b). Of course there is always the possibility that a foreground galaxy is located between us and the radio source. This would also explain why the optical spectrum shows no emission lines or signs of nuclear activity. Alternatively, it could

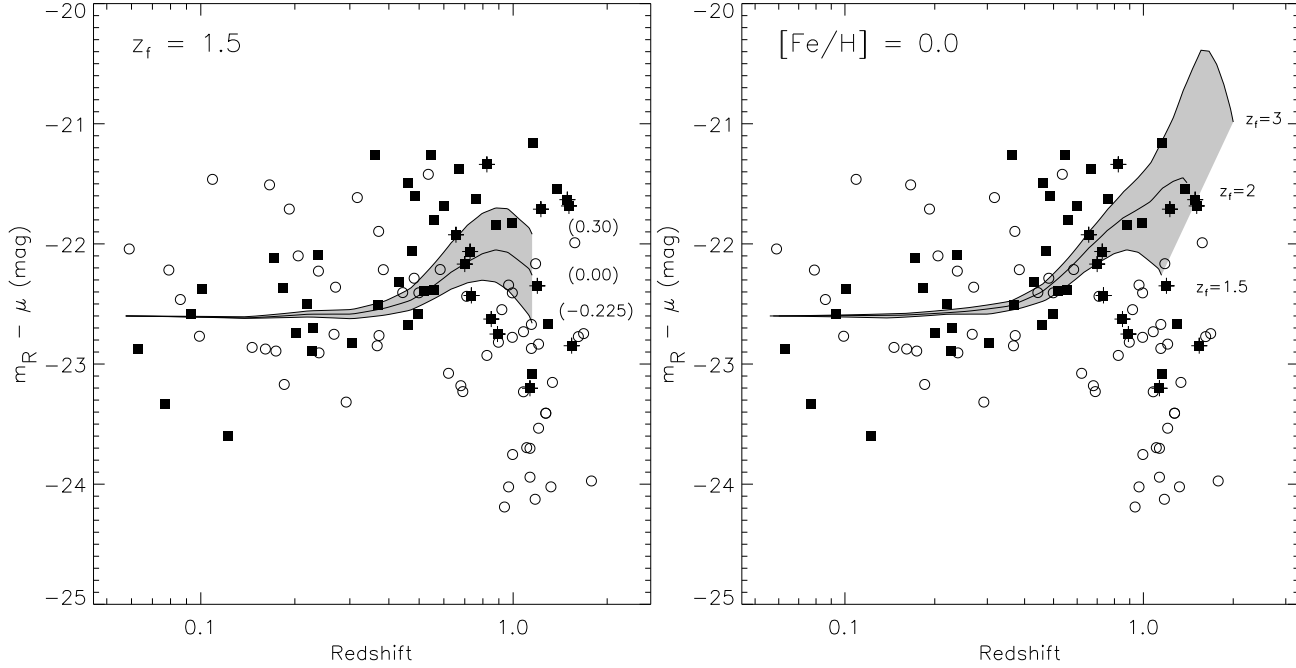


Fig. 2. (Left) Absolute magnitudes (without k-correction, $m_R - \mu$) for the combined samples of GPS galaxies (solid squares) and 3C galaxies (open circles). The grey shaded area is the modelled evolution, assuming a formation redshift of 1.5 and a range of metallicities from -0.225 to 0.30 . Evolutionary tracks for the extreme metallicities as well as one for solar metallicity are overplotted, with metallicity decreasing from the upper to the lower track. (Right) The same figure, except that the evolution models now vary in formation redshift and keep the metallicity fixed at solar. The evolutionary tracks are for a formation redshift of 1.5 (lower), 2 (middle) and 3 (upper).

be that the source is not a typical young powerful AGN, but some other object that happens to have a similar radio spectrum. Although PKS J1604–2223 is shown in Fig. 1, it is left out of any further analysis.

Now that the R -band Hubble relation is better sampled at $z \sim 1$ it is clear that the new data points systematically fall below the original fit (dotted line) of Snellen et al. (1996a). Since this relation is often used to estimate redshifts of GPS galaxies for which only photometric R -band data are available, it is valuable to determine a relation that holds for a larger redshift range, out to $z \approx 1.5$. We performed a linear least squares fit to the current data and found the relation:

$$m_{Rc} = 21.97 + 6.71 \times \log(z) \quad (2)$$

with a dispersion of 0.6 magnitudes. To estimate redshifts of GPS galaxies, this relation can be inverted to give:

$$z_{est} = 5.32 \cdot 10^{-4} \times (1.41)^{m_R}, \quad \sigma_z \approx 0.21 \times z_{est} \quad (3)$$

with σ_z the $1-\sigma$ uncertainty in the redshift estimate.

Furthermore the new data at $z \sim 1$ confirm that GPS galaxies are on average 1.0 magnitudes fainter in this redshift range than 3C radio galaxies, as was initially claimed by Snellen et al. (1996a). This agrees with the hypothesis that GPS galaxies are redder, due to the lack of the extra, blue light associated with the radio-optical alignment effect (Chambers, Miley & van Breugel 1987; McCarthy et al. 1987; Best, Longair & Röttgering 1997). The LRGs form a volume limited sample of the most luminous, intrinsically red galaxies out to $z \approx 0.55$. They are selected on the basis of colors and magnitudes, and

are thought to represent the most massive early type galaxies, many of which are classified as ‘Brightest Cluster Galaxies’. Fig. 1 shows that host galaxies of GPS radio sources have similar optical luminosities to LRGs, indicating that powerful young radio sources are hosted by the most massive early type galaxies. Note that the flattening of the distribution of LRGs at low redshift is probably due to the known problem that SDSS subtracts too high background levels for large sources, which can result in a magnitude difference of up to ~ 1 magnitude.

4.2. Absolute magnitudes

To study the cosmological evolution of GPS galaxies in more detail, we determined their absolute magnitudes M_{Rc} as a function of redshift. These can be calculated from the apparent magnitudes m_{Rc} , using (Hogg 2000):

$$\begin{aligned} m_{Rc} &= M_{Rc} + \mu + K \\ &= M_{Rc} + 5 \log\left(\frac{D_L}{10 \text{ pc}}\right) - 2.5 \log\left[\frac{L_{\lambda/(1+z)}}{(1+z)L_{\lambda}}\right] \end{aligned} \quad (4)$$

with μ the distance modulus, which depends, through the luminosity distance D_L , on the redshift of the source and on the assumed cosmology (we adopted the cosmological parameters as found by WMAP; Spergel et al. 2006). The last term, K , is the ‘k-correction’, which is required to convert the absolute magnitude to rest-frame R -band. This depends on the assumed spectral energy distribution (SED) of the source and is represented by the luminosity at the intrinsic wavelength $L_{\lambda/(1+z)}$ divided by that at the observed wavelength L_{λ} .

All variables in equation (4) are determined in a straightforward way from the observations and adopted cosmology, except for the k-correction. We therefore determined $m_R - \mu$ for each galaxy in the sample and determined a range of possible k-corrections, depending on the age and metallicity of the stellar population. For these we used the model galaxy SEDs by Worthey (1994). In figure (2) we show $m_R - \mu$ of the combined samples (see Sect. 4.1) of GPS galaxies (solid squares) and 3C galaxies (open circles) as a function of redshift. The three solid lines show the expected trend in $m_R - \mu$ for a stellar population with a formation redshift $z_f = 1.5$ and metallicities [Fe/H] of 0.3, 0.0, and -0.225 compared to solar. In figure (3) we show the same data, overplotted with the k-correction for a stellar population with solar metallicity and a range of formation redshifts of $z_f = 1.5, 2.0, \text{ and } 3.0$.

These figures show that the data are in best agreement with a recent formation redshift of $1.5 - 2.0$ (with a possible range of metallicities). However, we do not believe that the host galaxies really are that young, since GPS galaxies are always classified as early type galaxies, which are generally thought to have formed at higher redshifts ($z \sim 5$). In addition, Fig. 1 also indicates that GPS galaxies are old, massive, early type galaxies. Therefore we interpret this result as evidence for starburst activity and/or AGN induced light. We note that, although the optical/UV contribution from the alignment effect appears significantly smaller in GPS galaxies than for classical 3C radio galaxies, it does not exclude such AGN induced light being present at a low level. This extra blue light would brighten galaxies the most at high redshifts, where the *R*-band probes the rest-frame UV, and therefore could mimic a young stellar population and low formation redshifts. A thorough investigation using deep optical and infrared spectra will be needed to determine the possible contributions from the AGN and young starbursts to the overall galaxy spectrum.

Acknowledgements. This research has made use of observations collected at the ESO/Paranal Very Large Telescope and the ESO/La Silla 3.6m Telescope, and made use of the Vizier catalogue access tool, CDS, Strasbourg, France (Ochsenbein et al. 2000). This publication makes use of data products from the USNO-B1.0 Catalog and the Two Micron All Sky Survey, which is a joint project of the University of Massachusetts and the Infrared Processing and Analysis Center/California Institute of Technology, funded by the National Aeronautics and Space Administration and the National Science Foundation.

References

- Baum S.A., O’Dea C.P., Murphy D.W., de Bruyn A.G., 1990, A&A, 232, 19
- Best P.N., Longair M.S., Röttgering H.J.A., 1997, MNRAS, 292, 758
- Biretta J.A., Schneider D.P., Gunn J.E., 1985, AJ, 90, 250
- Chambers K.C., Miley G.K., van Breugel W., 1987, Nature, 329, 604
- Drinkwater M.J. et al., 1997, MNRAS, 284, 85
- de Koff S., Baum S.A., Sparks W.B. et al., 1996, ApJS, 107, 621
- de Vries W.H., Barthel P.D., Hes R., 1995, A&AS, 114, 259
- de Vries W.H., Barthel P.D., O’Dea C.P., 1997, A&A, 321, 105
- de Vries W.H., O’Dea C.P., Barthel P.D., Thompson D.J., 2000, A&AS, 143, 18
- Eales S.A., 1985, MNRAS, 213, 899
- Eisenstein D.J. et al., 2001, AJ, 122, 2267
- Fugmann W., Meisenheimer K., Roeser H.-J., 1988, A&AS, 75, 173
- Hambly N.C. et al., 2001, MNRAS, 326, 1279
- Hogg, D.W., 2000, astro-ph/9905116
- Irwin M., Maddox S., McMahon R., 1994, Spectrum, 2, 14
- McCarthy, P.J., van Breugel, W., Spinrad, H. Djorgovski, S., 1987, ApJ, 321, 29
- Murgia M., 2003, PASA, 20, 19M
- Ochsenbein F., Bauer P., Marcout J., 2000, A&AS 143, 221
- O’Dea C.P., Baum S.A., Morris G.B., 1990, A&A, 82, 261
- O’Dea C.P., Stanghellini C., Baum S.A., Charlott S., 1996, ApJ, 470, 806
- Otrupcek R., Wright A., 1991, PASA, 9, 170
- Owsianik I., Conway J.E., 1998, A&A, 337, 69
- Owsianik I., Conway J.E., Polatidis A.G., 1998, A&A, 336, L37
- Polatidis A.G., Conway J.E., 2003, PASA, 20, 69P
- Schombert J.M., Wallin J.F., & Struck-Marcell, C. 1990, AJ, 99, 497
- Snellen I.A.G., Bremer M.N., Schilizzi R.T., Miley G.K., van Ojik R., 1996a, MNRAS, 279, 1294
- Snellen I.A.G., Bremer M.N., Schilizzi R.T., Miley G.K., 1996b, MNRAS, 283, 123
- Snellen I.A.G., Schilizzi R.T., Bremer M.N. et al., 1999, MNRAS, 307, 149
- Snellen I.A.G., Lehnert M.D., Bremer M.N., Schilizzi R.T., 2002, MNRAS, 337, 981
- Spergel D.N. et al., 2006, submitted, “Three-Year Wilkinson Microwave Anisotropy Probe (WMAP) Observations: Implications for Cosmology”
- Stanghellini C., O’Dea C.P., Baum S.A., Laurikainen E., 1993, ApJS, 88, 1
- Stanghellini C., O’Dea C.P., Dallacasa D. et al., 1998, A&AS, 131, 303
- Stanghellini C., O’Dea C.P., Murphy D.W., 1999, A&AS, 134, 309
- Stern D., Dey A., Spinrad H. et al., 1999, AJ, 117, 1122
- Tschager W., Schilizzi R.T., Röttgering H.J.A., Snellen I.A.G., Miley G.K., 2000, A&A, 360, 887
- Vink J., Snellen I.A.G., Mack K.-H., Schilizzi R.T., 2006, MNRAS, 367, 928V
- Worthey G., 1994, ApJS, 95, 107
- Wright A., Otrupcek R., 1990, PKS Catalog

Appendix A: Comments on selected sources

PKS J0108–1201 The carbon line CIII] 1909 Å and the neon lines ([NeV] 3346 Å, [NeV] 3426 Å) are detected. By smoothing the spectrum with a boxcar of 20 pixels the MgII 2799 Å line is revealed as a broad (FWHM $\sim 250 \text{ Å} \sim 10^4 \text{ km/s}$) spectral feature, centered at $\sim 7100 \text{ Å}$.

PKS J0210+0419 Neither a continuum nor emission lines were detected for this object. This is consistent with the non-detection in the *R*-band (Snellen et al. 2002).

PKS J0401–2921 The spectrum shows very strong oxygen lines, weaker neon lines and the CaII K and H absorption features with a 4000 Å break.

PKS J0407–2757 The slit was tilted 45° so that the object North Western of the radio source (separation $\sim 2.5''$) was included. The North Western object shows many strong emission lines, where the South Eastern object shows [OII] 3727 Å and very weak neon lines. An *R*-band image of this source is shown in Fig. A.1.

PKS J0433–0229 The spectrum shows [OII] 3727 Å in

emission and the Ca II H, G-band, H γ , H β and MgI features in absorption.

PKS J1057+0012 This object was observed in photometric (1200 s) and spectroscopic (2700 s) mode on the ESO 3.6m Telescope. The images resulted in a new identification with a $m_{RC} = 22.5 \pm 0.3$ object, but the spectrum was not deep enough to determine a redshift for this source.

PKS J1109+1043 This radio source has erroneously been identified with a $m_{RC} = 20.5$ object. It was already noted (Snellen et al. 2002) that there was a large offset between the radio and optical position. Our observations resulted in an identification with a much fainter object ($m_{RC} = 22.6 \pm 0.3$) at the radio position. The S/N of the spectrum (2700 s on the 3.6m Telescope) was too low to see spectral features.

PKS J1135-0021 This radio source has erroneously been identified with a star ($m_{RC} = 16.5$). In our long slit spectrum we found, at a distance of about 2.4'' from the typical stellar spectrum, a faint AGN spectrum from which we determined a redshift of 0.975. From the acquisition image we also estimated the magnitude of the object: $m_{RC} = 21.9 \pm 0.4$.

PKS J1203+0414 Spectroscopic observations of this object show a typical quasar spectrum with broad carbon and magnesium lines and the object should therefore be removed from the sample of GPS galaxies.

PKS J1345-3015 The spectrum shows a strong [OII] 3727 Å line, the CII] 2326 Å, [NeV] 3426 Å and [NeIII] 3869 Å lines and a very broad MgII feature.

PKS J1352+1107 The [OII] 3727 Å line, the neon emission lines and the CaII K and H absorption features are detected.

PKS J1506-0919 Spectroscopic observations of this object show a typical quasar spectrum with broad carbon and mag-

nesium lines and the object should therefore be removed from the sample of GPS galaxies.

PKS J1556-0622 Only one emission line is detected, so only a tentative redshift could be determined. We assumed the line to be [OII] 3727 Å, because of the resemblance between this spectrum and those of PKS J2339-0604 and PKS J2212+0152, and the absence of viable alternatives.

PKS J1648+0242 The spectrum shows very weak [OII] 3727 Å and neon emission lines, but strong CaII K and H absorption features, the G-band and the 4000 Å break.

PKS J1734+0926 The [OII] 3727 Å and [NeIII] 3869 Å emission lines are weak, but the H γ and CaII K and H absorption features, the G-band and the 4000 Å break are strong.

PKS J2212+0152 The [OII] 3727 Å emission line is strong and the MgII 2798 Å and neon lines are weak.

PKS J2339-0604 The spectrum shows a strong [OII] 3727 Å line and weak CII] 2326 Å, MgII 2798 Å and [NeIII] 3869 Å lines.

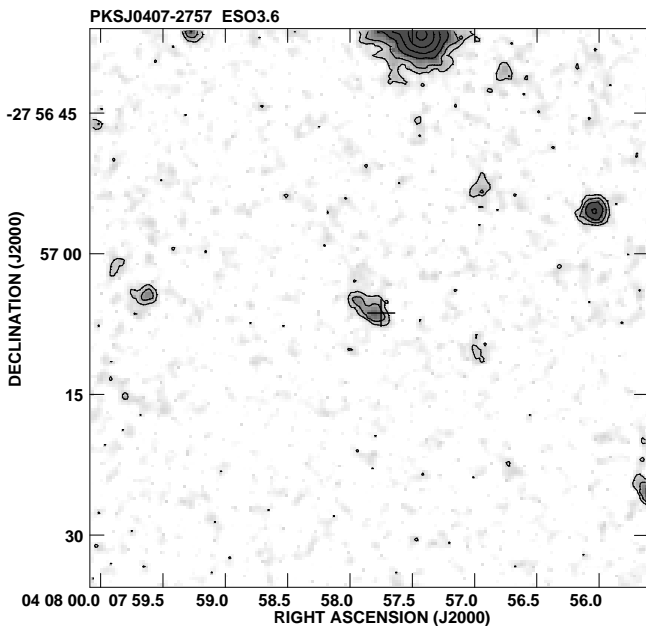


Fig. A.1. R-band image of PKS J0407-2757 taken from Snellen et al. (2002). The GPS radio source is located in the South Eastern object, as indicated with the plus sign. Most of the line emission originates from the object North Western of the radio source.

Table B.1. The radio and optical properties of objects in the southern/equatorial sample of GPS galaxies.

IAU name	Other name	Radio position (J2000)		m_{RC} (mag)	z	$S_{2.7\text{GHz}}$ (Jy)	ν_{peak} (GHz)	S_{peak} (Jy)	Ref. m_R	Ref. z	Comm.
J0022+0014	4C+00.02	00 22 25.48	+ 00 14 56.0	18.10 ± 0.20	0.305	1.94	0.6	3.1	3	3	A
J0108-1201	B0105-122	01 08 13.20	-12 00 50.3	22.39 ± 0.06	1.539	0.52	1.0	0.9	2	1	
J0206-3024	B0204-306	02 06 43.26	-30 24 58.2	21.00 ± 0.50		0.58	0.5	0.9	14		
J0210+0419	B0208+040	02 10 44.52	+04 19 35.4	K_s 18.3 ± 0.2		0.56	0.4	1.3	1		
J0210-2213	B0207-224	02 10 10.05	-22 13 36.6	23.52 ± 0.13	1.491	0.86	1.5	1.1	2	1	
J0242-2132	B0240-217	02 42 35.87	-21 32 26.2	17.10 ± 0.50	0.314	0.97	1.0	1.3	14	12	
J0323+0534	4C+05.14	03 23 20.27	+05 34 11.9	19.20 ± 0.50		1.60	0.4	7.1	14		
J0401-2921	B0359-294	04 01 21.50	-29 21 26.1	21.00 ± 0.20	0.656	0.58	0.4	1.0	1	1	
J0407-3924	B0405-395	04 07 34.43	-39 24 47.2	20.40 ± 0.50	0.474	0.52	0.4	1.4	14	1	
J0407-2757	B0405-280	04 07 57.94	-27 57 05.1	21.14 ± 0.04	0.728	0.93	1.5	1.4	2	1	
J0433-0229	4C-02.17	04 33 54.90	-02 29 56.0	19.10 ± 0.50	0.530	1.04	0.4	3.0	14	1	
J0441-3340	B0439-337	04 41 33.80	-33 40 03.6	22.50 ± 0.40		0.88	1.5	1.2	1		
J0457-0848	B0454-088	04 57 20.24	-08 49 05.2	20.30 ± 0.50	0.516	0.58	0.4	1.0	14	1	
J0503+0203	B0500+019	05 03 21.20	+02 03 04.6	21.0 ± 0.20	0.583	2.46	2.5	2.5	5	5	A
J0943-0819	B0941-080	09 43 36.86	-08 19 32.0	17.50 ± 0.20	0.228	1.73	0.4	4.2	10	11	A
J0913+1454	B0910+151	09 13 35.00	+14 54 20.1	22.90 ± 0.50		0.54	0.6	1.1	1		
J1044-2712	B1042-269	10 44 37.63	-27 12 18.6	22.80 ± 0.40		0.55	1.5	0.8	1		
J1057+0012	B1054+004	10 57 15.78	+00 12 03.7	22.30 ± 0.30		0.58	0.4	1.6	1		
J1109+1043	B1107+109	11 09 46.04	+10 43 43.4	22.60 ± 0.30		0.80	0.5	2.4	1		
J1110-1858	B1107-187	11 10 00.45	-18 58 49.2	19.60 ± 0.20	0.497	0.65	1.0	0.9	9	13	
J1120+1420	4C+14.41	11 20 27.81	+14 20 55.0	20.10 ± 0.10	0.362	1.50	0.4	3.7	5	5	A
J1122-2742	B1120-274	11 22 56.41	-27 42 48.2	23.00 ± 0.50		0.74	1.4	0.8	1		
J1135-0021	4C-00.45	11 35 12.96	-00 21 19.5	21.90 ± 0.40	0.975	0.76	0.4	2.9	1	1	
J1203+0414	B1200+045	12 03 21.95	+04 14 17.7	18.80 ± 0.50	1.221	0.52	0.4	1.4	14	1	E
J1345-3015	B1343-300	13 45 51.52	-30 15 04.1	21.20 ± 0.20	1.132	0.56	0.4	2.5	1	1	
J1347+1217	4C+12.50	13 47 33.36	+12 17 24.2	15.20 ± 0.20	0.122	3.88	0.4	8.8	3	3	A
J1350-2204	B1347-218	13 50 14.33	-22 04 43.7	20.93 ± 0.05	0.700	0.72	0.4	1.4	2	1	
J1352+0232	B1349+027	13 52 30.68	+02 32 47.7	20.00 ± 0.50	0.607	0.78	0.4	2.0	14	1	
J1352+1107	4C+11.46	13 52 56.37	+11 07 07.7	21.00 ± 0.20	0.891	0.78	0.4	3.6	1	1	
J1447-3409	B1444-339	14 47 19.69	-34 09 16.2	21.00 ± 0.10	0.851	0.50	0.5	1.0	14	1	
J1506-0919	B1503-091	15 06 03.05	-09 19 12.5	19.70 ± 0.50	1.486	0.87	0.6	1.6	14	1	E
J1521+0430	4C+04.51	15 21 14.51	+04 30 20.0	22.10 ± 0.11	1.296	2.30	1.0	5.4	7	11	A
J1543-0757	B1540-077	15 43 01.69	-07 57 03.6	17.40 ± 0.10	0.172	1.21	0.4	1.7	6	6	C
J1546+0026	B1543+005	15 46 09.50	+00 26 24.6	20.10 ± 0.20	0.556	1.24	0.6	2.2	3	6	C
J1548-1213	B1545-120	15 48 12.97	-12 13 31.8	21.88 ± 0.13	0.883	1.45	0.4	3.7	2	2	
J1556-0622	4C-06.43	15 56 13.99	-06 22 37.8	22.20 ± 0.13	(1.195)	0.77	0.4	2.4	2	1	
J1600-0037	B1557-004	16 00 00.91	-00 37 23.3	-		0.54	1.0	1.2	2		D
J1604-2223	B1601-222	16 04 01.45	-22 23 41.3	18.75 ± 0.10	0.141	0.57	0.6	1.0	6	2	
J1640+1220	4C+12.60	16 40 47.96	+12 20 02.1	21.36 ± 0.20	1.150	1.48	0.4	3.7	2	2	
J1648+0242	4C+02.43	16 48 31.79	+02 42 46.0	22.10 ± 0.30	0.824	0.61	0.4	3.4	1	1	
J1734+0926	B1732+094	17 34 58.38	+09 26 57.8	20.80 ± 0.10	0.735	1.08	1.0	1.1	6	1	B
J2011-0644	B2008-068	20 11 14.22	-06 44 03.6	21.18 ± 0.04	0.547	2.09	1.4	2.6	2	2	A
J2058+0540	4C+05.78	20 58 28.84	+05 42 50.7	23.40 ± 0.30	1.381	0.65	0.4	3.1	8	8	
J2123-0112	B2121-014	21 23 39.12	-01 12 34.3	23.30 ± 0.10	1.158	0.64	0.4	2.0	4	3	
J2130+0502	B2128+048	21 30 32.88	+05 02 17.5	22.21 ± 0.07	0.990	3.12	1.0	4.8	2	11	A
J2151+0552	B2149+056	21 51 37.88	+05 52 13.0	20.20 ± 0.20	0.740	1.01	5.0	1.2	4	11	A, E
J2212+0152	4C+01.69	22 12 37.97	+01 52 51.7	22.0 ± 0.20	1.126	1.80	0.4	4.6	5	1	A
J2325-0344	B2322-040	23 25 10.23	-03 44 46.7	23.50 ± 0.20	1.509	0.91	1.4	1.2	10	1	B
J2339-0604	4C-06.76	23 37 11.95	-06 04 12.4	22.91 ± 0.20	1.227	0.80	0.4	3.8	2	1	

Comments: (A) also in the sample of > 1 Jy GPS sources from Stanghellini et al. (1998); (B) also in the sample of de Vries et al. (1997) (C) also in the sample of de Vries et al. (2000); (D) near a bright star, no magnitude; (E) radio source is optically identified with a quasar; will be excluded from the sample.

References: (1) this paper; (2) Snellen et al. (2002); (3) Snellen et al. (1996a); (4) O’Dea, Baum & Morris (1990); (5) de Vries et al. (1995); (6) de Vries et al. (2000). (7) Biretta, Schneider & Gunn (1985); (8) Stern et al. (1999); (9) Fugmann, Meisenheimer & Roeser (1988); (10) Stanghellini et al. (1993); (11) Stanghellini et al. (1998); (12) Otrupcek & Wright (1991); (13) Drinkwater et al. (1997); (14) Digitized Sky Survey II; APM catalogue (Irwin et al. 1994); SuperCosmos Sky Surveys (Hambly et al. 2001).

Appendix B: Tables and figures

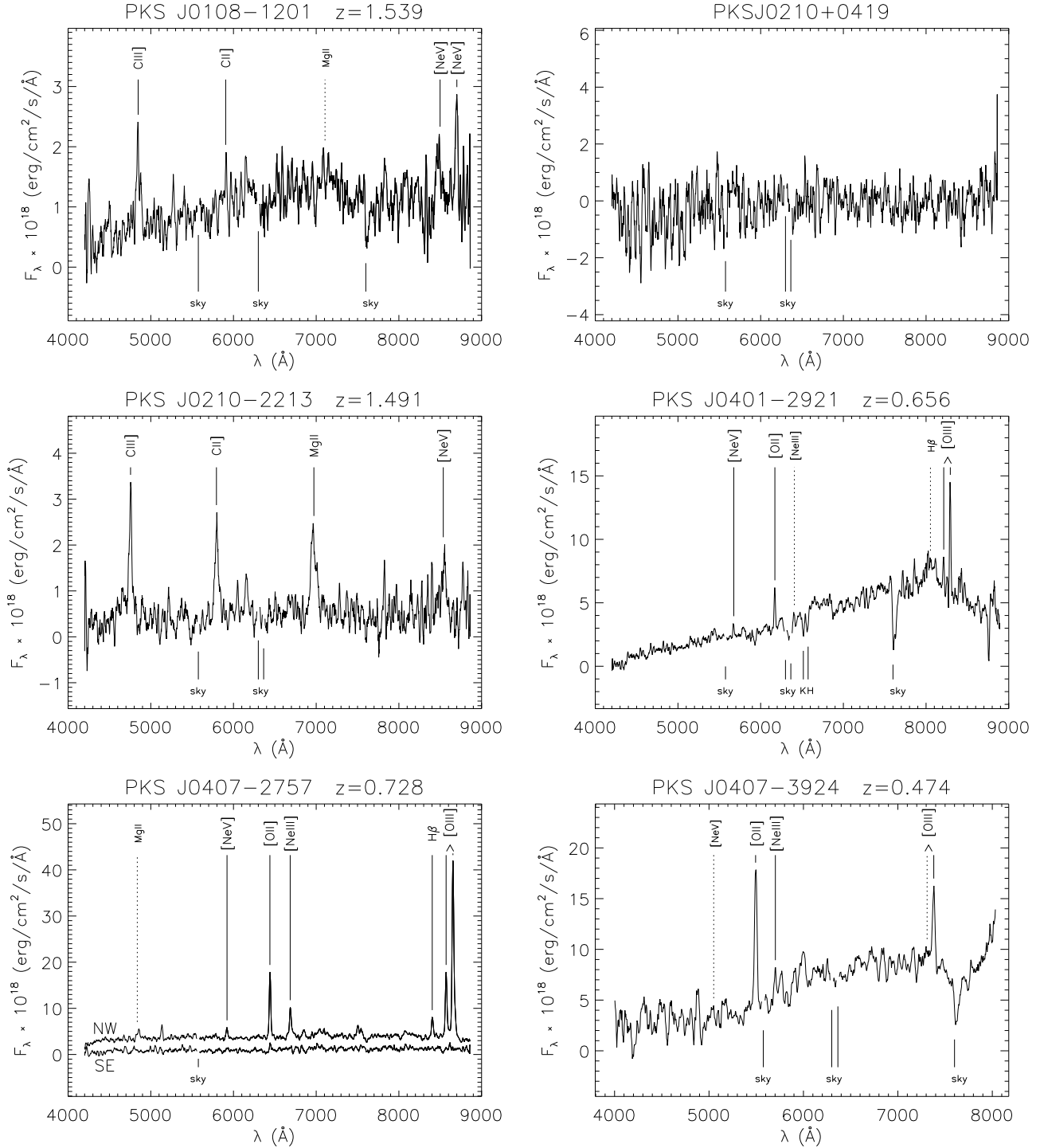


Fig. B.1. Spectra from the ESO Very Large Telescope and ESO 3.6m Telescope of 24 objects in the sample. From 21 spectra, a redshift could be deduced, which is indicated at the top. Labeled are emission and absorption lines that were used to determine the redshift (drawn lines) and wavelengths where other common emission lines are expected (dotted lines). Regions where the night sky emission lines are strong have been omitted. These regions are indicated, as well as the 7600 Å sky absorption feature.

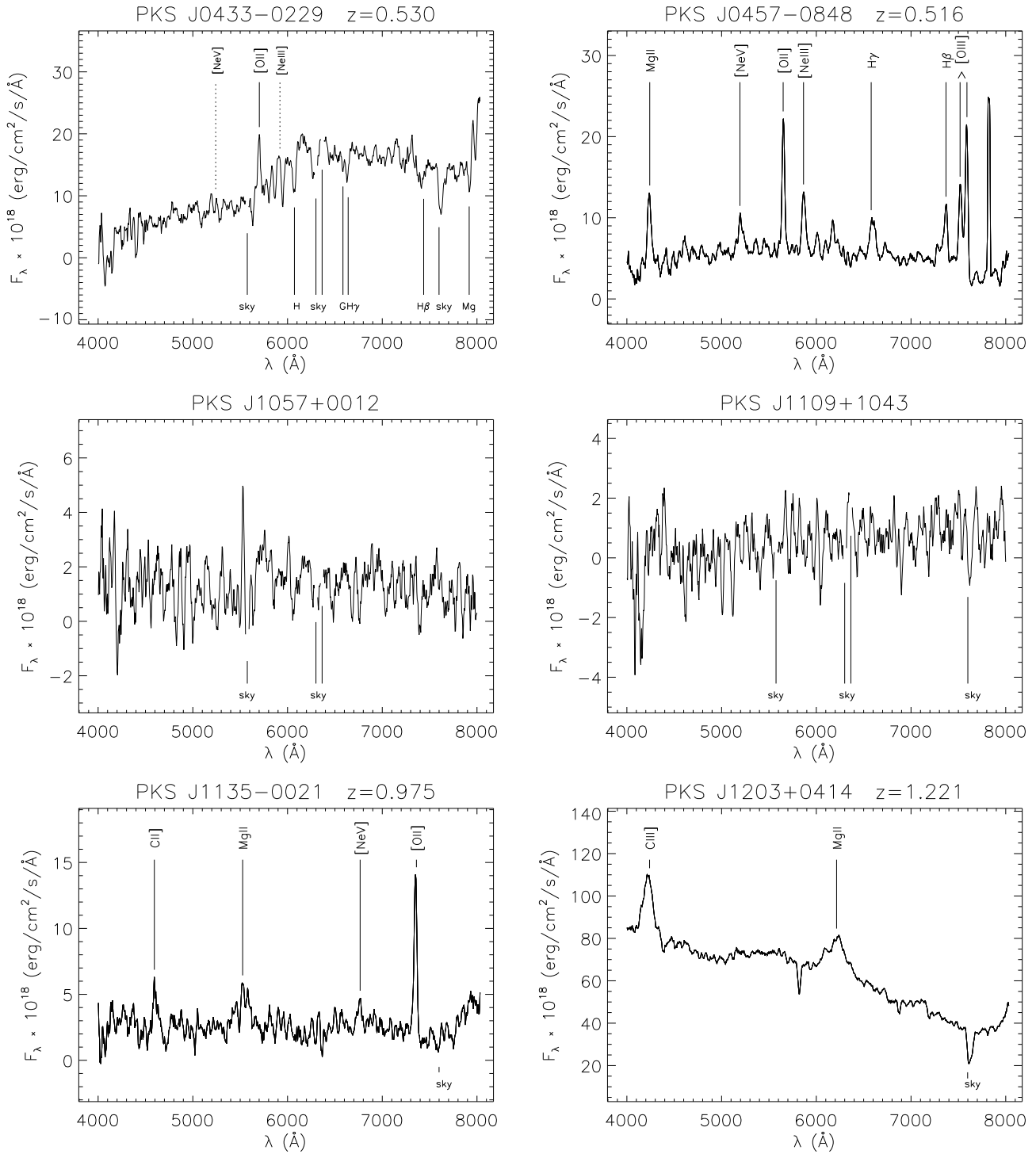


Fig. B.1. continued

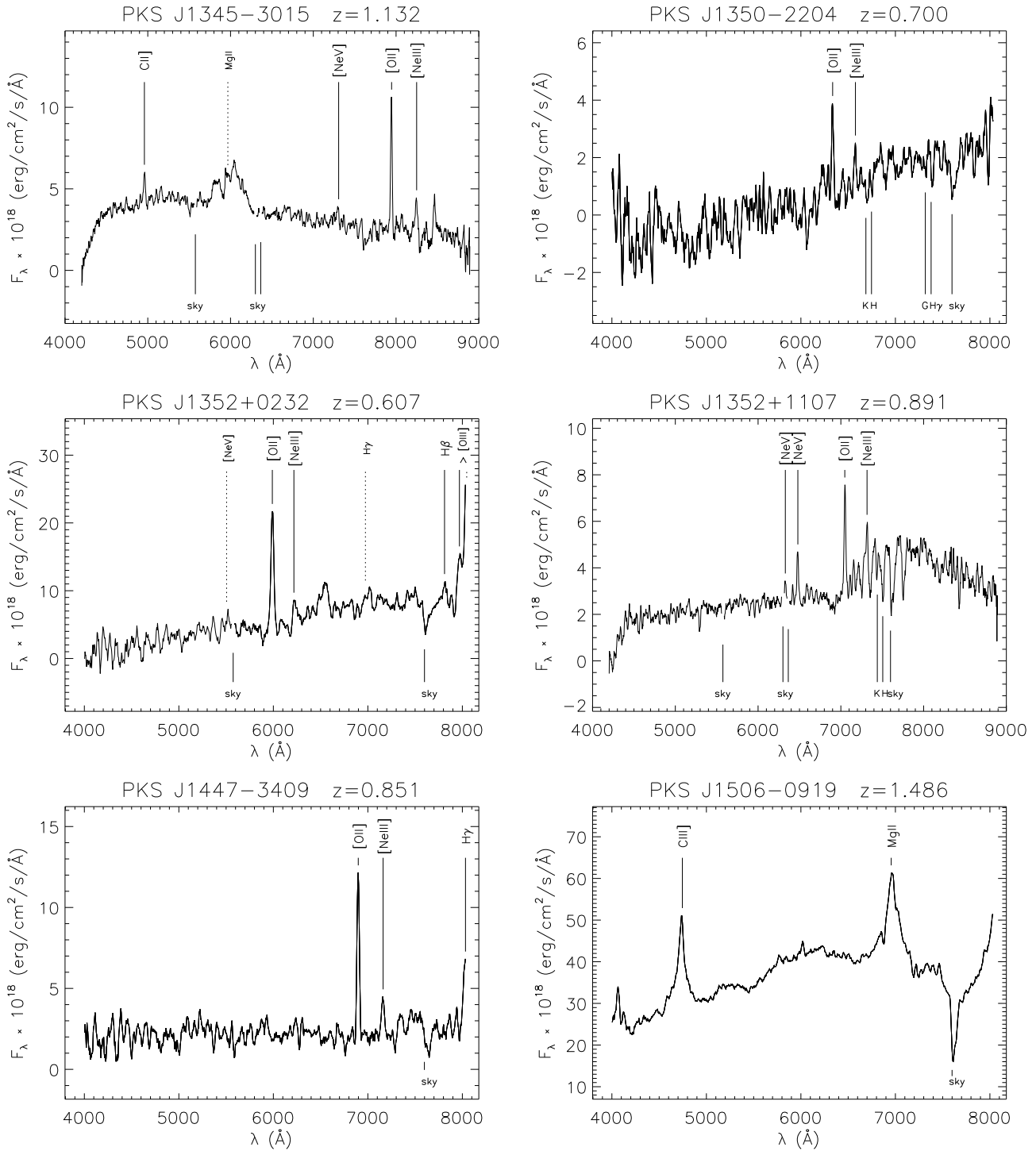


Fig. B.1. continued

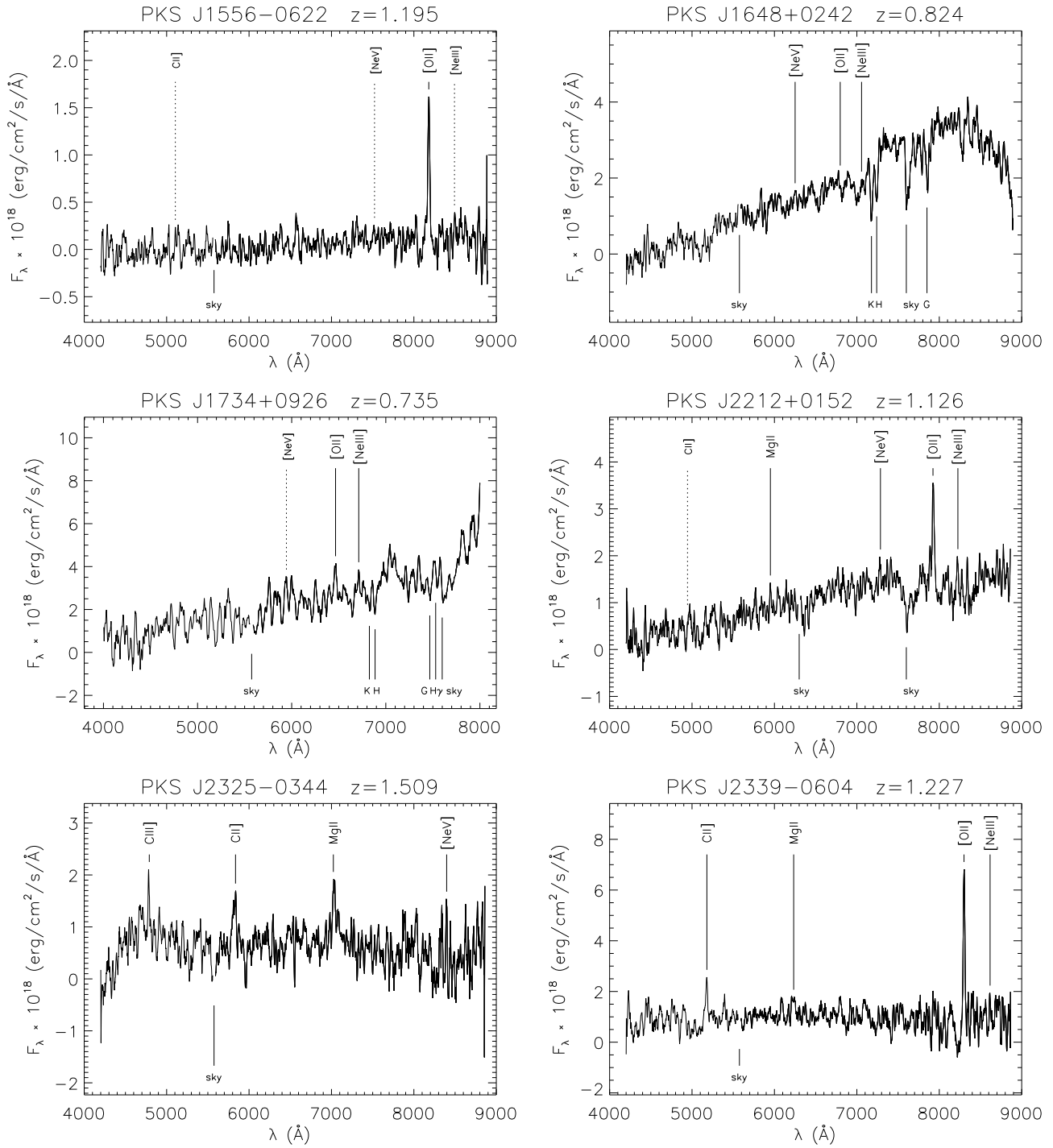


Fig. B.1. continued

Table B.2. Details of the spectroscopic observations.

Object name	t (s)	Telescope	Spectral feature			z
			Species	λ_{rest} (Å)	λ_{obs} (Å)	
PKS J0108–1201	1800	ESO VLT				1.539 ± 0.001
			CIII]	1909	4845	1.538
			CII]	2326	5911	1.541
			[NeV]	3346	8488	1.537
			[NeV]	3426	8700	1.539
PKS J0210+0419	1800	ESO VLT				
PKS J0210–2213	1800	ESO VLT				1.491 ± 0.003
			CIII]	1909	4757	1.492
			CII]	2326	5799	1.493
			MgII	2798	6964	1.489
			[NeV]	3426	8553	1.497
PKS J0401–2921	1800	ESO VLT				0.656 ± 0.001
			[NeV]	3426	5672	0.656
			[OII]	3727	6170	0.656
			CaII K	3934	6518	0.657
			CaII H	3969	6562	0.653
			[OIII]	4959	8212	0.656
			[OIII]	5007	8290	0.656
PKS J0407–2756 North West	1800	ESO VLT				0.728 ± 0.001
			[NeV]	3426	5920	0.728
			[OII]	3727	6442	0.728
			[NeIII]	3869	6687	0.728
			H β	4861	8404	0.729
			[OIII]	4959	8571	0.728
			[OIII]	5007	8654	0.728
PKS J0407–2756 South East	1800	ESO VLT				0.729 ± 0.001
			[NeV]	3426	5929	0.731
			[OII]	3727	6442	0.729
PKS J0407–3924	2700	ESO 3.6m				0.474 ± 0.001
			[OII]	3727	5496	0.475
			[NeIII]	3869	5700	0.473
			[OIII]	5007	7379	0.474
PKS J0433–0229	1200	ESO 3.6m				0.530 ± 0.001
			[OII]	3727	5496	0.530
			CaII H α	3969	6071	0.530
			G-band α	4304	6584	0.530
			H γ α	4340	6634	0.529
			H β α	4861	7411	0.525
			MgI α	5175	7921	0.531
PKS J0457–0848	2700	ESO 3.6m				0.516 ± 0.001
			MgII	2798	4238	0.515
			[NeV]	3426	5195	0.516
			[OII]	3727	5653	0.517
			[NeIII]	3869	5865	0.516
			[SII]	4072	6174	0.516
			H γ	4340	6582	0.517
			[OIII]	4363	6618	0.517
			H β	4861	7373	0.517
			[OIII]	4959	7521	0.517
			[OIII]	5007	7589	0.516
PKS J1057+0012	2700	ESO 3.6m				
PKS J1109+1043	2700	ESO 3.6m				

Table B.2. Details of the spectroscopic observations, continued.

Object name	t (s)	Telescope	Spectral feature			z
			Species	λ_{rest} (Å)	λ_{obs} (Å)	
PKS J1135–0021	1800	ESO 3.6m				0.975 ± 0.002
			CII]	2326	4593	0.975
			MgII	2798	5531	0.977
			[NeV]	3426	6769	0.976
PKS J1203+0414	1200	ESO 3.6m	[OII]	3727	7351	0.972
						1.221 ± 0.004
			CIII]	1909	4230	1.216
			MgII	2798	6225	1.225
PKS J1345–3015	1800	ESO VLT				1.132 ± 0.001
			CII]	2326	4960	1.132
			[NeV]	3426	7297	1.130
			[OII]	3727	7944	1.132
PKS J1350–2204	2700	ESO 3.6m	[NeIII]	3869	8248	1.132
						0.700 ± 0.002
			[OII]	3727	6333	0.699
			[NeIII]	3869	6572	0.699
PKS J1352+0232	1800	ESO 3.6m	CaII K _a	3934	6707	0.705
			CaII H _a	3969	6752	0.701
			G-band _a	4304	7317	0.700
			H γ _a	4340	7390	0.703
PKS J1352+1107	1800	ESO VLT				0.607 ± 0.001
			[OII]	3727	5990	0.607
			[NeIII]	3869	6215	0.606
			H β	4861	7813	0.607
PKS J1352+1107	1800	ESO VLT	[OIII]	4959	7968	0.607
						0.891 ± 0.001
			[NeV]	3346	6329	0.892
			[NeV]	3426	6478	0.891
PKS J1447–3409	5400	ESO 3.6m	[OII]	3727	7050	0.892
			[NeIII]	3869	7319	0.892
			CaII K	3934	7434	0.890
			CaII H	3969	7508	0.892
PKS J1506–0919	2700	ESO 3.6m				0.851 ± 0.001
			[OII]	3727	6898	0.851
			[NeIII]	3869	7161	0.851
PKS J1506–0919	2700	ESO 3.6m	H γ	4340	8047	0.854
						1.486 ± 0.003
			CIII]	1909	4740	1.483
PKS J1556–0622	1800	ESO VLT	MgII	2798	6966	1.490
						1.195 ± 0.001
PKS J1556–0622	1800	ESO VLT	[OII]	3727	8182	1.195
						0.824 ± 0.001
PKS J1648+0242	1800	ESO VLT	[NeV]	3426	6252	0.825
			[OII]	3727	6777	0.818
			[NeIII]	3869	7069	0.827
			CaII K	3934	7176	0.824
PKS J1734+0926	5400	ESO 3.6m	CaII H	3969	7242	0.825
			G-band	4305	7856	0.825
						0.735 ± 0.001
			[NeV]	3426	5938	0.733
PKS J1734+0926	5400	ESO 3.6m	[OII]	3727	6468	0.735
			[NeIII]	3869	6713	0.735

Table B.2. Details of the spectroscopic observations, continued.

Object name	t (s)	Telescope	Spectral feature			z	
			Species	λ_{rest} (Å)	λ_{obs} (Å)		
PKS J2212+0152	1800	ESO VLT	CaII K _α	3934	6829	0.736	
			CaII H _α	3969	6884	0.735	
							1.126 ± 0.001
			MgII	2798	5955	1.128	
			[NeV]	3426	7280	1.125	
			[OII]	3727	7926	1.127	
PKS J2325−0344	1800	ESO VLT	[NeIII]	3869	8219	1.124	
							1.509 ± 0.002
			CIII]	1909	4781	1.505	
			CII]	2326	5837	1.510	
			MgII	2798	7029	1.512	
			[NeV]	3346	8394	1.109	
PKS J2339−0604	3600	ESO VLT				1.227 ± 0.001	
			CII]	2326	5181	1.226	
			MgII	2798	6230	1.227	
			[OII]	3727	8300	1.227	
			[NeIII]	3869	8617	1.226	